

Some SIF's evaluations by Dual BEM for 3D cracked plates

R. Citarella ^{a,*}, A. Soprano ^b

^a Department of Mechanical Engineering, University of Salerno, via Ponte Don Melillo, 84084 Fisciano, Salerno, Italy

^b Department Aerospace and Mechanical Engineering, 2nd University of Naples, Italy

* Corresponding author: E-mail address: rcitarella@unisa.it

Received in revised form 15.07.2006; accepted in final form 30.10.2006

Analysis and modelling

ABSTRACT

Purpose: of this work is to provide a numerical assessment of 3D crack problems with linear and non-linear loading conditions.

Design/methodology/approach: Single-Domain Boundary Element Method and in particular Dual Boundary Element Method (DBEM) is adopted. The method, implemented in a commercial code, uses both the conventional Displacement Integral Equation and the less commonly used Traction Integral Equation. It relies on the use of discontinuous elements to model the cracks, whose Stress Intensity Factors (SIF's) are calculated by means of the Crack Opening Displacement method (COD).

Findings: SIF's on a circular quadrant crack and a rectangular through crack, initiated from a hole, have been evaluated with reference to single and two hole plates undergoing different linear and non-linear loading conditions. Such complex geometric and loading condition is worked out very efficiently and accurately by DBEM that is strongly recommended for this kind of application in alternative to FEM.

Research limitations/implications: Further improvement in the BEASY code will be necessary in order to lighten computational times. The presented analysis provide the basis for further development related to crack propagation analysis and residual strength assessment.

Practical implications: The methodology proposed will enable a significant reduction of the experimental effort.

Originality/value: The solution of a 3d crack assessment under non linear loading conditions with the possibility of checking the accuracy of the DBEM results against FEM calculus and other approaches (recalled in literature) in order to have a clear assessment of the possible industrial applications with related approximations involved.

Keywords: Numerical techniques; DBEM; Contact analysis; 3D crack corner crack; Through crack

1. Introduction

Damage Tolerance is used in the design of many types of structures, such as bridges, military ships, commercial aircraft, space vehicle and merchant ships. It requires accurate prediction of fatigue crack growth under service conditions and typically this is accomplished with the aid of a numerical code. Many aspects of fracture mechanics are more complicated in practice than in two-dimensional laboratory tests, textbook examples, or overly

simplified computer programs. Load spectrum, threshold effects, environmental conditions, microstructural effects, small crack effects, Multiple Site Damage (MSD) conditions, material parameters scatter, mixed loading conditions and complex three dimensional geometry, all complicate the process of predicting fatigue crack growth in real word applications.

This paper focuses on some of these complications: three dimensional crack assessment under complex stress state. In particular, a series of test have been designed and implemented to evaluate the SIF's prediction capabilities for the Dual Boundary

Element Method (DBEM) [1-2], as implemented in the commercial code BEASY [3]. With such methodology, the geometry of the test specimen and the shapes of crack fronts are not restricted to the simplified configurations found in the libraries of many commercial codes.

2. Dual Boundary Element Method

There follows a summary of the Single-Domain Boundary Element Method and in particular the Dual Boundary Element Method, for the numerical evaluation of linear elastic crack problems using boundary integral equations with discontinuous elements. The method, very powerful in particular for crack propagation problems, uses both the conventional Displacement Integral Equation (the free term of which involves displacements at the source point) and the less commonly used Traction Integral Equation (the free term of which involves tractions at the source point). Actually, the displacement equation alone does not provide a viable method for single domain analysis of general crack problems, because of the stiffness matrix ill-conditioning (there is not a sufficient number of independent equations). This drawback can be circumvented adopting two independent equations on the two crack edges.

2.1. Boundary Integral Equations (BIE)

Define spatial coordinates x_i (subscript $i=1,2,3$), with source point x_i^* . Displacement $u_i(x)$ and traction $t_i(x)$ on the boundary S of a three-dimensional solid are related by the displacement BIE (1) and traction BIE (2) (three components $j=1,2,3$), for a source point on a smooth boundary S where the summation convention is assumed for repeated suffices:

$$\frac{1}{2} \delta_{ij} u_j(x^*) + \int_S T_{ij}(x^*, x) u_j(x) dS(x) - \int_S U_{ij}(x^*, x) t_j(x) dS(x) = 0 \quad (1)$$

$$\frac{1}{2} t_i(x^*) - n_i(x^*) \int_S D_{ij}(x^*, x) t_k(x) dS(x) + n_i(x^*) \int_S S_{kij}(x^*, x) u_k(x) dS(x) = 0 \quad (2)$$

This is a limiting form of the BIE characterised by a source point interior to the boundary S . The kernel functions $T_{ij}(x^*, x)$ and $D_{kij}(x^*, x)$ are $O(r^{-2})$ singular while $S_{kij}(x^*, x)$ is $O(r^{-3})$ singular. The

two symbols \int_S^- , $\int_S^=$ stand respectively for the Cauchy and Hadamard principal value integrals.

In the displacement and traction equation, there arise apparently singular terms due to the presence of the source point on the boundary. Provided that certain continuity conditions hold for the surface variables (displacement and traction) at the source point, no singularities actually exist and the integral equations are well defined.

2.2. Discontinuous elements

Application of conventional Boundary Element Method with continuous element to the hypersingular traction equation fails due to the unsuitable representation of the surface displacement and traction at the nodal source points. The numerical solutions will not converge unless the assumed form of displacement and traction on the boundary element adjoining the source point comply with the following conditions: displacement and traction assumed on the boundary elements must be respectively C^1 and C^0 -continuous at the boundary source point. The necessary conditions for the existence of the principal value integrals obtained in the derivation of the dual boundary integral equations impose restrictions on the discretization. Actually, in the traction equation the continuity requirements of the Hadamard principal value integral are satisfied (in a simple way) only by discontinuous elements, since all the nodes are internal points of the element where a continuous differential approximation is defined. Moreover, using the traction equation, the geometry smoothness requirement at a collocation point is implicitly satisfied by the discontinuous element.

2.3. Crack modelling

The general modelling strategy can be summarised as follows:

- the traction equation (2) is applied for collocation on one of the crack boundaries;
- the displacement equation (1) is applied for collocation on the opposite crack boundary and remaining boundaries;
- the crack boundaries are discretized with discontinuous boundary elements;
- continuous quadratic boundary element are used along the remaining boundaries of the problem domain, except at the intersection between a crack and an edge, where discontinuous or semi-discontinuous elements are required, in order to avoid nodes at the intersection.

3. Stress Intensity Factors (SIF's)

Discontinuous quadratic boundary elements are used along the crack front, and values of stress intensity factors (SIF's) are derived from the crack opening displacement method (COD) on such elements, by using the BEASY code, well suited for 3D SIF's evaluation and automatic crack propagation.

4. Example solutions

A large square plate contains one or two cracked holes; its overall sizes are: $-B < x_1 < +B$, $-H < x_2 < +H$, $-h/2 < x_3 < h/2$, as shown in Fig. 1-2. Values of tensile modulus $E=72000 \text{ N/mm}^2$ and Poisson's ratio $\nu = .3$ are assumed. The hole radius is $R=2.0 \text{ mm}$ and, in the two hole case, the hole pitch is $P=20.0 \text{ mm}$. The plate dimensions $2B$ and $2H$ are chosen sufficiently large so as to simulate an infinite panel and the plate thickness is $h=1.6 \text{ mm}$.

Two structural configurations are considered:

A single hole plate, with a circular quadrant surface crack (Fig.1) of radius $a_1=1.2$ mm or $a_1=0.8$ mm and with a panel size of $2B=2H=80$ mm (adequate in order to approximate as infinite the plate with less than 1.5% SIF's variation);

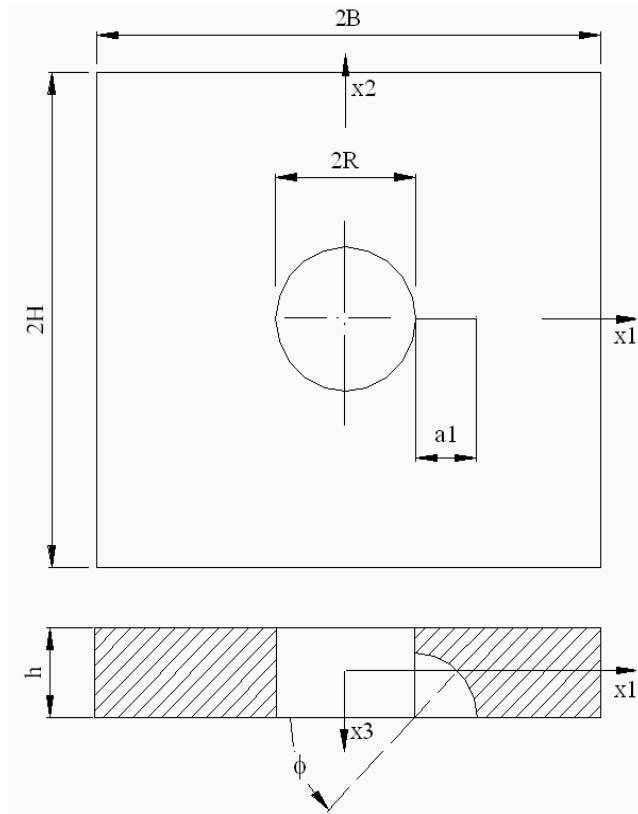


Fig. 1. One hole plate with circular crack at a hole

2. A two hole plate with a quadrant crack of radius $a_1=0.8$ mm and a nearby through-crack emanating from an adjacent hole (Fig.2) of length $a_2=8.0$ mm, with a panel size of $2B=2H=160$ mm (adequate in order to approximate as infinite the plate with less than 1.5% SIF's variation).

The loading cases considered for the one hole plate are (Fig.3):

- uniform remote tension $S=100$ N/mm² applied as tractions on one end surface, whilst the other end surface is suitably constrained. SIF's values for the quadrant crack ($a_1=1.2$ mm) are normalised by $K_0 = S\sqrt{\pi \cdot a_1 / Q}$, where $Q=2.464$ [4].
- uniform remote bending $\sigma_{22} = S(2x_3/h)$ each applied as tractions t_2 acting on the end surface $x_2=+H$ whilst the other end surface is suitably constrained. SIF's values for quadrant crack ($a_1=1.2$ mm) are normalised as above;
- momentum of magnitude $M=F \cdot 3.2=5120$ N*mm ($F=1600$ N), applied by means of a tilted pin, with the contact area modelled by gap elements. SIF's values for the quadrant crack ($a_1=0.8$ mm) are normalised by $K_0 = S\sqrt{\pi \cdot a_1 / Q}$, where $Q=2.464$ [4]. In this load case the tension S is the hole bearing stress and is calculated as $S=F/(2 \cdot R \cdot h)=250$ N/mm².

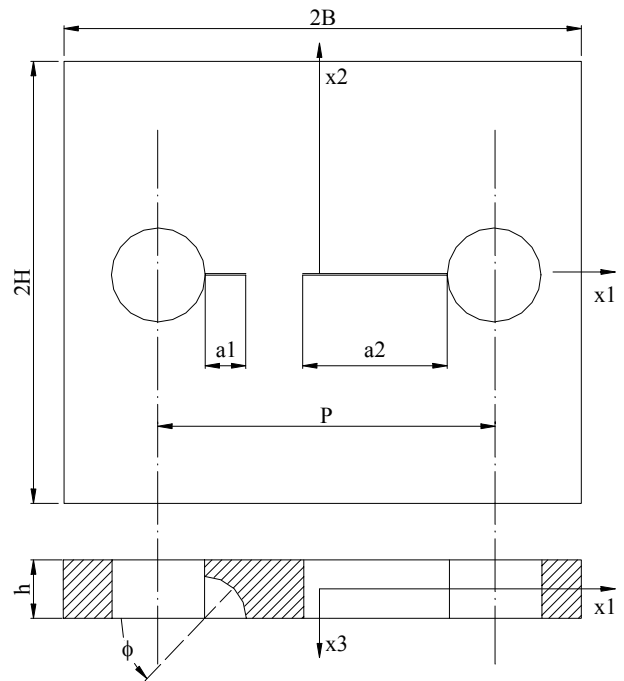


Fig. 2. Two hole plate with quadrant and through cracks

The loading case considered for the two hole plate is (Fig.4): pin load of magnitude $F=1600$ N, applied as body load in each pin (made of the same plate material) of the two-hole plate, with the contact area modelled by gap elements. SIF's values for the quadrant crack are normalised by $K_0 = S\sqrt{\pi \cdot a_1 / Q}$, where $Q=2.464$ [4]. SIF's values for the through crack are normalised by $K_0 = S\sqrt{\pi \cdot a_2}$. In this load case the tension S is the hole bearing stress and is calculated as $S = F / (2 \cdot R \cdot h) = 250$ N/mm² ($F=1600$ N).

4.1. One hole plate results

For one-hole plate, in the case of uniform remote tension, tridimensional numerical solutions have been obtained using a total of about 990 linear elements, as in Fig.5, except on the cracks where "reduced" quadratic elements (8-noded elements) have been used in any case.

This mesh corresponds to 6252 degrees of freedom (dof's). Increasing the order of the elements to "reduced" quadratics (7533 dof) around the crack, produced a slight SIF's variation (less than 2%) while run-times increased significantly. Negligible changes (less than 1%) in the solution were produced by setting up the element subdivision option, applied to the most refined mesh adopted, capable to augment the number of Gauss quadrature points in quasi-singular integrations. Using an increased number of subdivisions in the angular and radial direction had a negligible effect on the results (moreover it would be possible to reduce the number of crack elements without affecting significantly the results). Normalised SIF's (K_I / K_0 , $K_0=124$ Nmm^{-3/2}) for the quadrant crack, $a_1=1.2$ mm, are given in

Fig. 6. The mesh on the crack is based on 8 uniform divisions in the angular direction and 6 divisions in the radial direction as illustrated, together with Von Mises stresses for traction case, in Fig. 7a-b.

The same remarks hold for the bending case where the same mesh as above has been adopted but now it is necessary a p-convergence analysis up to quadratic elements (9-noded elements), in order to get good convergence results. Von Mises stress on the overall plate and in particular around the hole are illustrated in Fig. 8a-b. Normalized SIF's for the quadrant crack (K_I/K_0 , $K_0=124 \text{ Nmm}^{-3/2}$) are presented in Fig. 9. Von Mises stress and crack mesh are depicted in Fig. 10.

For tilted-pin case, the mesh adopted is based on 1190 elements varying from linear to quadratic in a p-convergence study. Such mesh is well evident from Fig. 11a-d, where deformed plots, representative of the stress state, are magnified by a factor of 15. The analysis is non linear and an iterative-incremental procedure is adopted. In Fig. 12-14 normalised SIF's (K_I/K_0 , K_{II}/K_0 , K_{III}/K_0) are depicted. In this case there is a mixed load condition even if the mode I of load is prevailing.

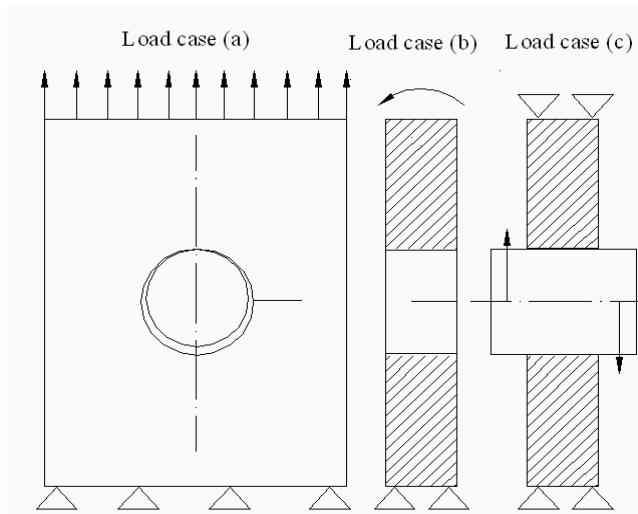


Fig. 3. Loading conditions for the one hole plate

This mesh corresponds to 6252 degrees of freedom (dof's). Increasing the order of the elements to "reduced" quadratics (7533 dof) around the crack, produced a slight SIF's variation (less than 2%) while run-times increased significantly. Negligible changes (less than 1%) in the solution were produced by setting up the element subdivision option, applied to the most refined mesh adopted, capable to augment the number of Gauss quadrature points in quasi-singular integrations. Using an increased number of subdivisions in the angular and radial direction had a negligible effect on the results (moreover it would be possible to reduce the number of crack elements without affecting significantly the results). Normalised SIF's (K_I/K_0 , $K_0=124 \text{ Nmm}^{-3/2}$) for the quadrant crack, $a_1=1.2 \text{ mm}$, are given in Fig. 6. The mesh on the crack is based on 8 uniform divisions in the angular direction and 6 divisions in the radial direction as illustrated, together with Von Mises stresses for traction case, in Fig. 7a-b.

The same remarks hold for the bending case where the same mesh as above has been adopted but now it is necessary a p-convergence analysis up to quadratic elements (9-noded elements), in order to get good convergence results. Von Mises stress on the overall plate and in particular around the hole are illustrated in Fig. 8a-b. Normalized SIF's for the quadrant crack (K_I/K_0 , $K_0=124 \text{ Nmm}^{-3/2}$) are presented in Fig. 9. Von Mises stress and crack mesh are depicted in Fig. 10.

For tilted-pin case, the mesh adopted is based on 1190 elements varying from linear to quadratic in a p-convergence study. Such mesh is well evident from Fig. 11a-d, where deformed plots, representative of the stress state, are magnified by a factor of 15. The analysis is non linear and an iterative-incremental procedure is adopted. In Fig. 12-14 normalised SIF's (K_I/K_0 , K_{II}/K_0 , K_{III}/K_0) are depicted. In this case there is a mixed load condition even if the mode I of load is prevailing.

4.2. Two hole plate results

For two hole plate, the boundary element mesh used for the quadrant crack corresponds to 6 uniform divisions in the angular direction and 4 divisions in the radial direction, whilst for the through crack it corresponds to 6 uniform divisions in x_3 direction and 5 divisions in x_1 direction. The plate boundary mesh is easily obtained.

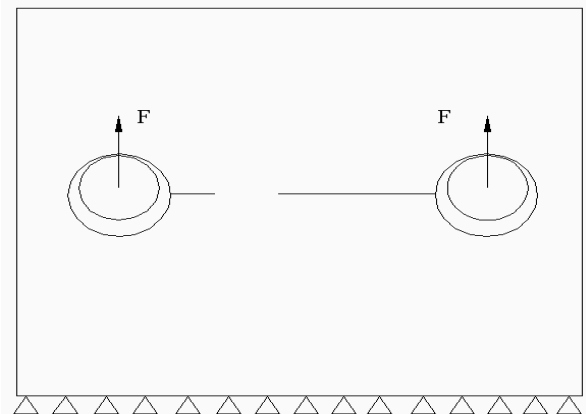


Fig. 4. Loading condition for the two hole plate

For pin-loading case, linear elements have been used throughout the plate surface, except in the zone surrounding the two holes, including the two loaded pins, modelled with "reduced" quadratic elements. In this contact problem, modelled with gap elements on the interface area, the analysis is non-linear because of a changeable contact area with a gradually increasing load and it is worked out by an iterative-incremental procedure. In Fig. 15a-c are illustrated normal tractions on pin-hole contact area (it is evident they are zero in the disconnected part). Normalized SIF's for the quadrant cracks are depicted in Fig. 16a, and those for the through cracks in Fig. 16b. In Fig. 17 Von Mises stress are well evident around the cracks whose opening in the deformed plate is showed too.

The plate boundary mesh is illustrated in Fig. 18.

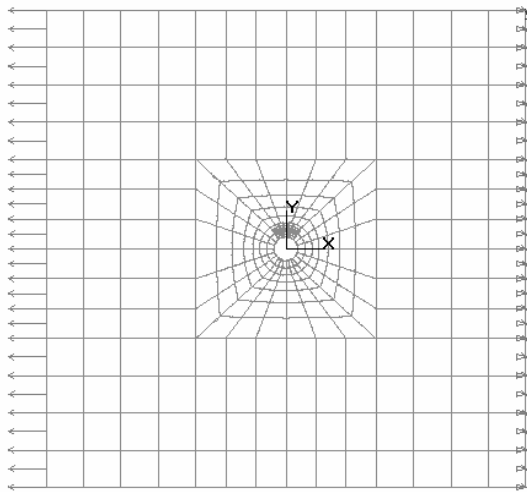


Fig. 5. Overall boundary mesh for the one hole plate

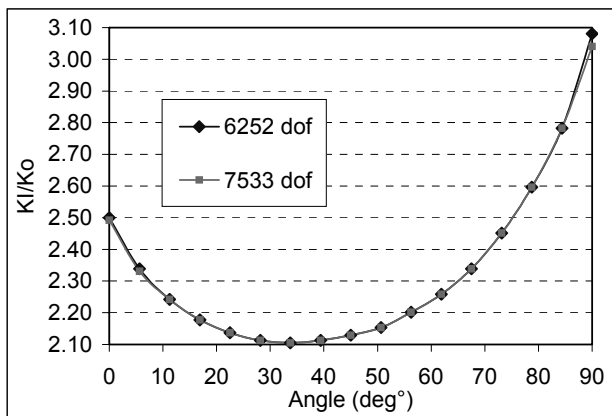


Fig. 6. Normalized SIF's for the one hole plate in traction case

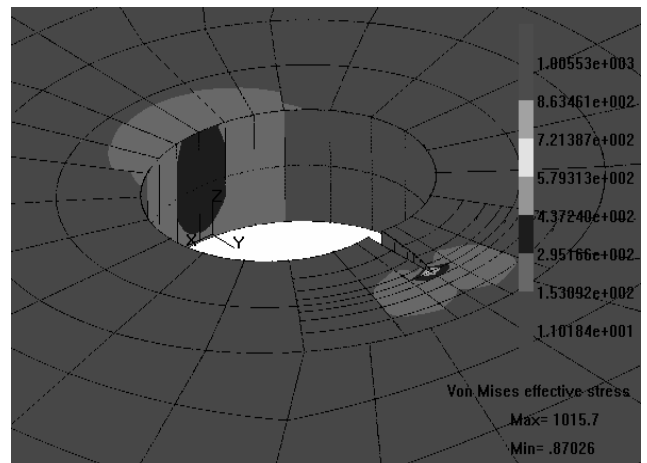


Fig. 7b. Close-up of the hole mesh and Von Mises stress state

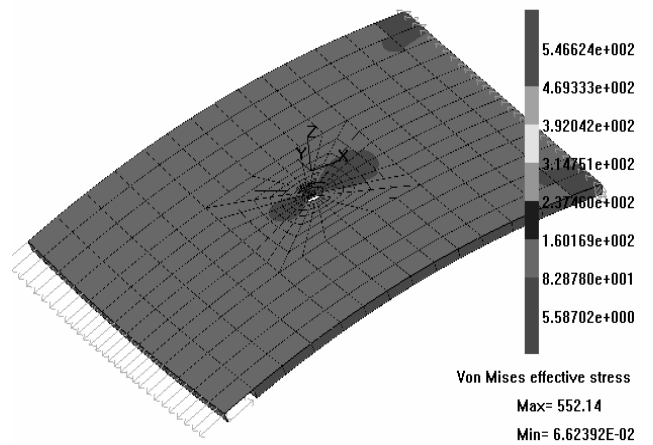


Fig. 8a. Overall stress state on the one hole plate deformed plot, in bending case

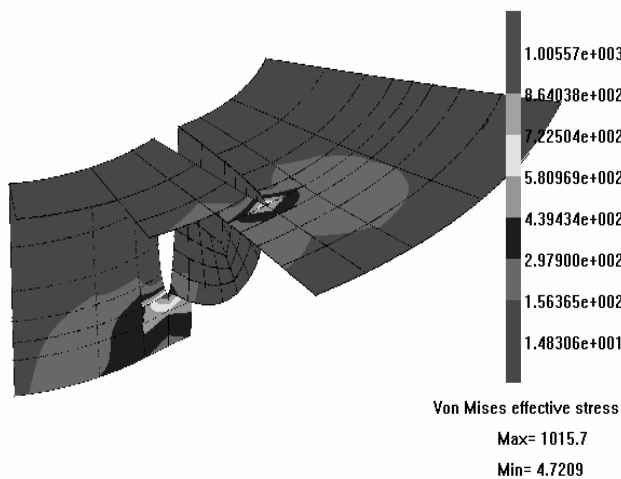


Fig. 7a. Close-up of the crack element mesh and stress state

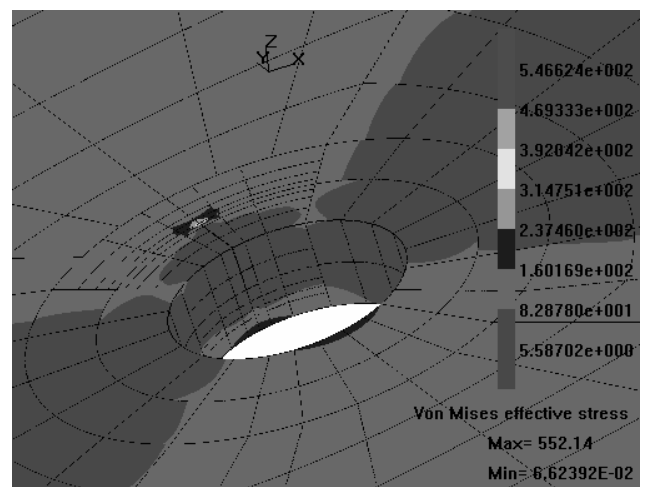


Fig. 8b. Close-up of the stress state around the hole (R=2mm)

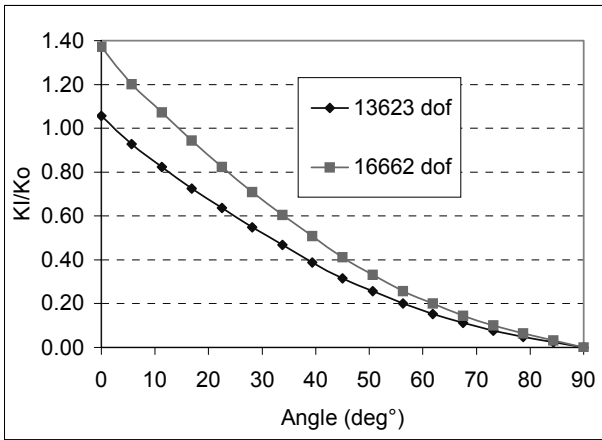


Fig. 9. Normalized SIF's (K_I / K_0 with $K_0=124 \text{ Nmm}^{-3/2}$) for the one hole plate in bending case

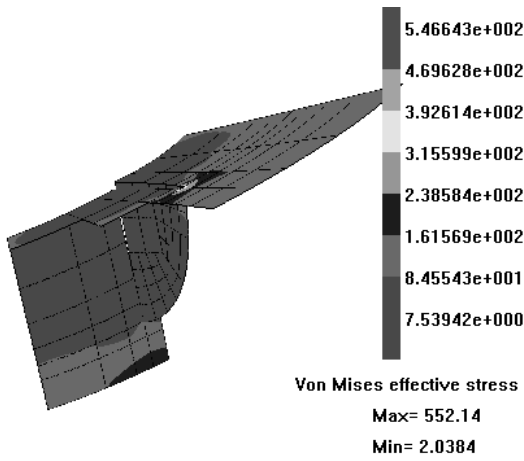


Fig. 10. Stress state around the crack ($a_1=1.2$), in bending case

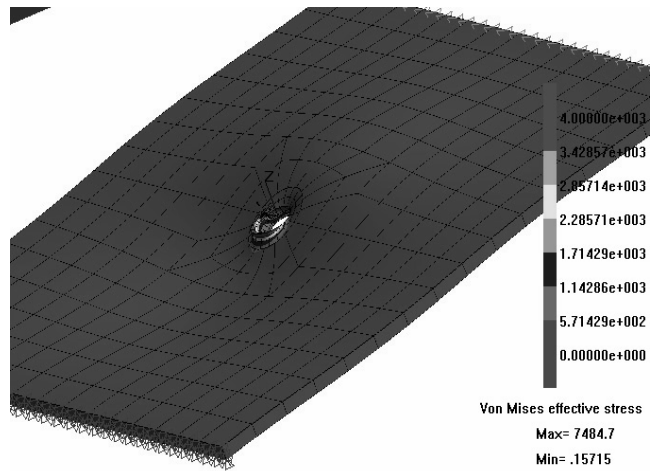


Fig. 11b. Stress state on a deformed plot, for a clamped plate undergoing momentum

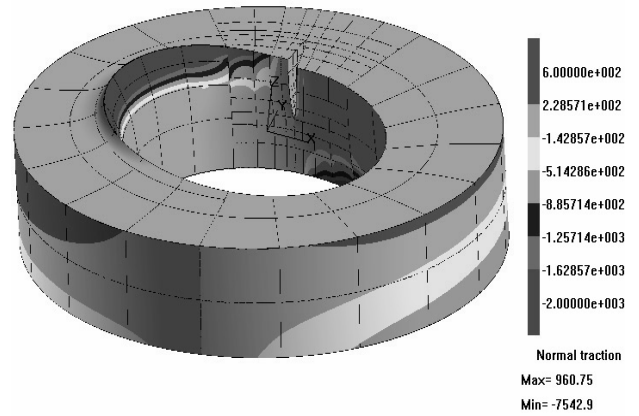


Fig. 11c. Close-up of the hole contact pressure on one hole plate deformed plot

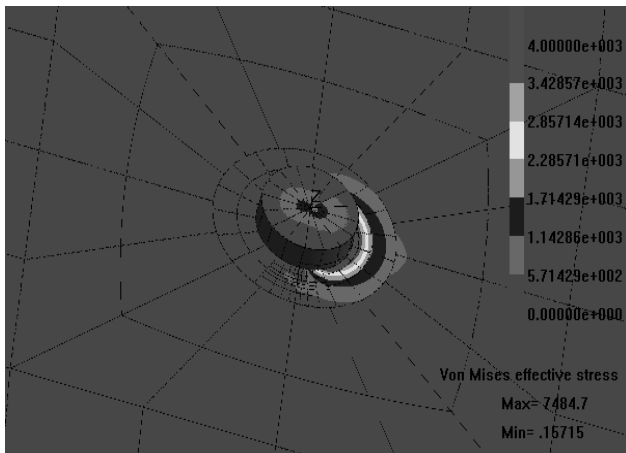


Fig. 11a. Close up of the stress state for a tilted pin ($M=5120 \text{ Nmm}$, $a_1=0.8 \text{ mm}$) in the one hole plate

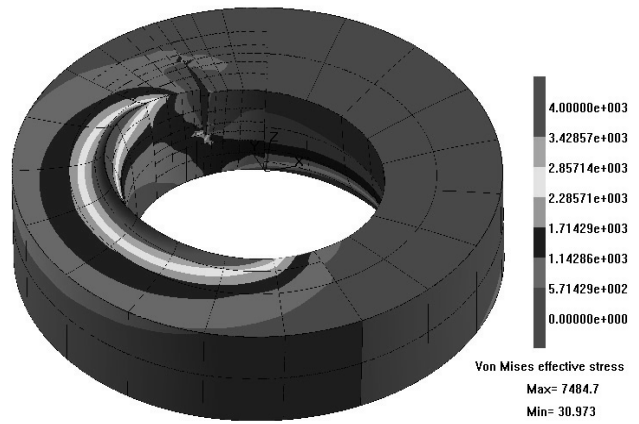


Fig. 11d. Close-up of the hole surface contact stress on one hole plate deformed plot

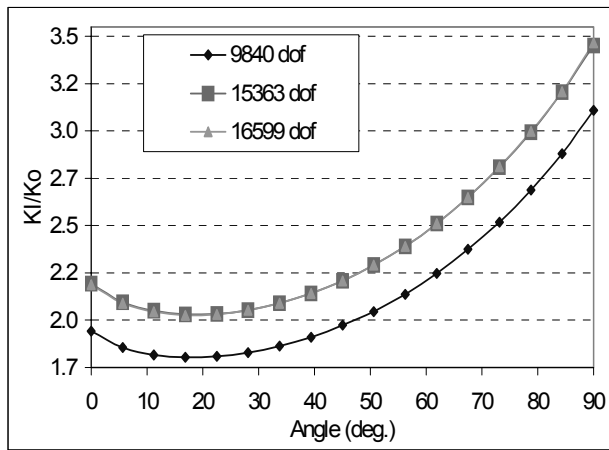


Fig. 12. Normalized SIF's (KI/Ko , $Ko=252 \text{ Nmm}^{-3/2}$, $a_1=0.8\text{mm}$) in tilted pin case

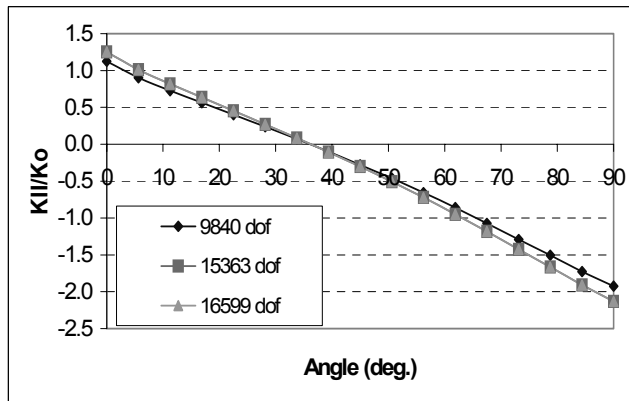


Fig. 13. Normalized SIF's (KII/Ko , $Ko=252 \text{ Nmm}^{-3/2}$, $a_1=0.8\text{mm}$) in tilted pin case

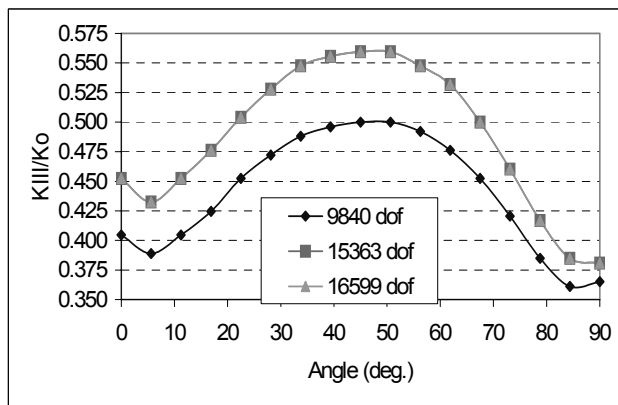


Fig. 14. Normalized SIF's (KI/Ko , $Ko=252 \text{ Nmm}^{-3/2}$, $a_1=0.8\text{mm}$) in tilted pin case

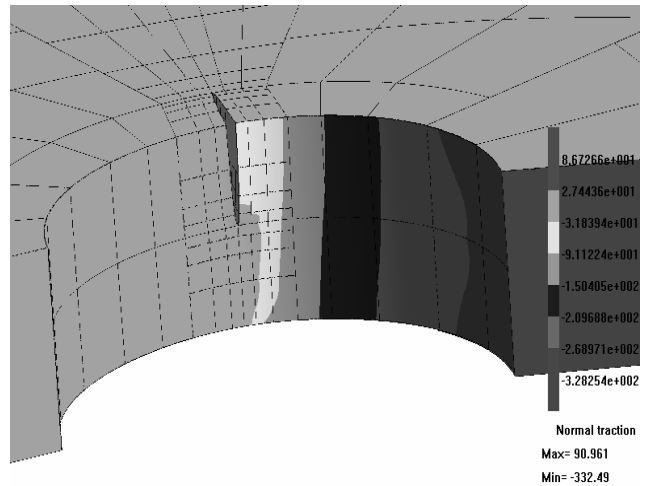


Fig. 15a. Hole bearing traction on the deformed contact area for the pin-loaded two hole plate

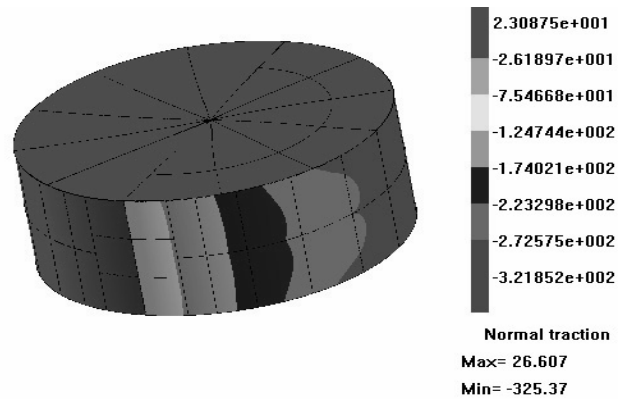


Fig. 15b. Pin bearing traction on the deformed contact area for the pin-loaded two hole plate

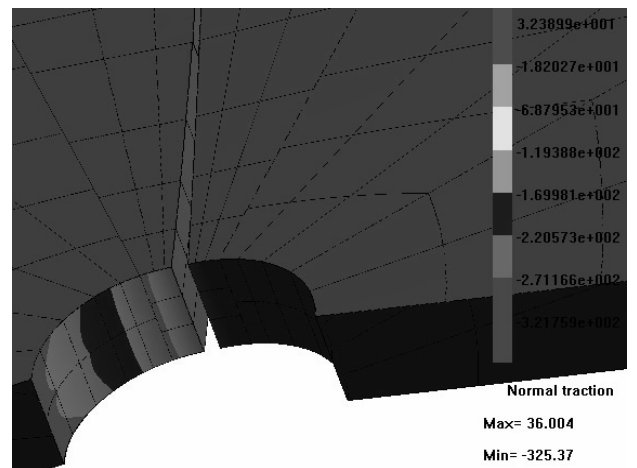


Fig. 15c. Pin bearing traction on the deformed contact area for the pin-loaded two hole plate

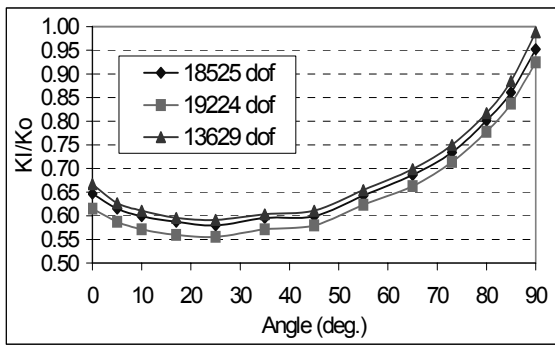


Fig. 16a. Normalized SIF's ($K_0=252 \text{ Nmm}^{-3/2}$) for quadrant crack of the pin-loaded plate

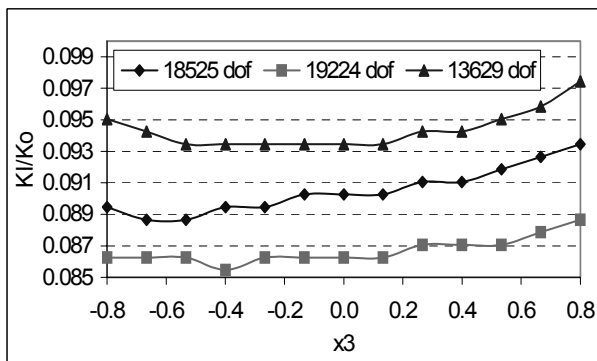


Fig. 16b. Normalized SIF's ($K_0=1252 \text{ Nmm}^{-3/2}$) for through crack of the pin-loaded plate

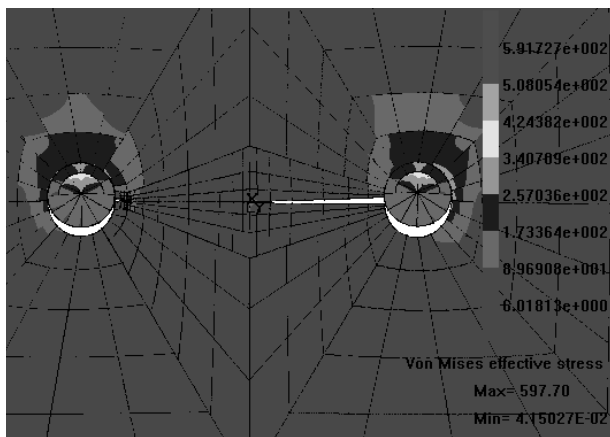


Fig. 17. Stress state around the deformed holes of the pin-loaded plate ($F=1600 \text{ N}$ on each pin)

4.3. Multi region formulation

Since the procedures developed for FEM generally assume a particular type of matrix, i.e. symmetric, positive definite (SPD),

sparse with small bandwidth, new solution strategies are required to solve the different types of matrix produced by BEM.

In the construction of large, complex models it is often more economical to split the model into smaller simpler sub-models. These sub-models or regions, which may also have different material properties, are modelled independently and then joined together along an interface. This strategy leads to an overall system matrix which has a blocked, sparse and unsymmetric character. This characteristic of multi-region formulation significantly extends the range of problems that can be solved, due to the large savings in storage and CPU calculations, required to solve the matrix, compared with the case of a fully populated matrix. However, the sparsity of such matrices is of a different type than that of FEM matrices. This has led to research being concentrated on the direct method for solving matrices, characterised by the factorisation of the system matrix by Gauss elimination or by Choleski's method. As a matter of fact a direct method is implemented in BEASY code for system matrices resolution.

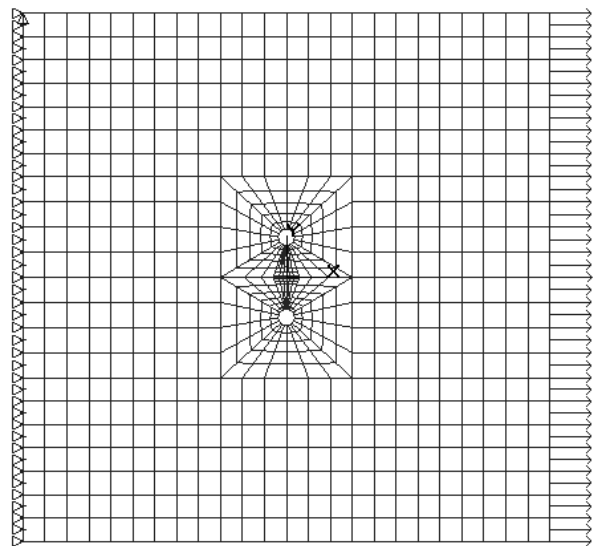


Fig. 18. Overall boundary element mesh used for the two hole plate, in bending case

5. Conclusions

In conclusion some further remarks are due with regard to the opportunity, with a DBEM procedure, to model the zone surrounding the cracks with discontinuous elements, in such a way to simplify the meshing process and without loss of accuracy. Moreover it has been possible to reduce run times and storage required, by zoning the whole plate in an adequate number of parts (paying attention to number consecutively the adjacent zones, in order to maximize benefits). Cubic elements have also been tried in the zone surrounding the cracks but without any improvement in accuracy. A satisfactory agreement of the results has been obtained with a relatively small modelling effort, compared with the partners of SMAAC project (a BRITE-

EURAM European project entitled Structural Maintenance of Ageing Aircraft) [5-8] and other authors [9].

Further improvement in the BEASY code will be necessary in order to lighten computational times.

The presented detailed analysis aimed at SIF's assessment on a crack of a given length provide the basis for further development related to crack propagation analysis [10-11] and residual strength assessment [12]. The crack propagation simulation for specimens made of specific materials (described in [13-16]) and for a shaft-hub coupling [17] is currently under development.

References

- [1] Y. Mi, M.H. Aliabadi, "Three-dimensional crack growth simulation using BEM", *Computers & Structures*, Vol 52, No 5 (1994) 871-878.
- [2] A. Apicella, R. Citarella, R. Esposito, "Sulla previsione della propagazione per fatica di cricche multiple tramite elementi di contorno discontinui", *Proceedings of XXIII Convegno Nazionale AIAS*, Rende, 1994.
- [3] A.C. Neves, R.A. Adey, J.M.W. Baynham and S.M. Niku, "Automatic 3D crack growth using BEASY", *Proceedings of BEM 19 Conference*, 819-827, Computational Mechanics Publications, Southampton, U.K. (1997).
- [4] P.W. Tan, J.C. Newman Jr, C.A. Bigelow "Three-dimensional finite element analysis of corner cracks at stress concentration", *Engineering Fracture Mechanics* 55 (1996) 502-505.
- [5] JPM Goncalves, PMST de Castro. Contribution to the numerical modeling of the interaction between a corner crack and a through crack, SMAAC-WP-2.0-XX-1.0/IDMEC, Brite-Euram Project No. BE95-1053, 1997.
- [6] JPM Goncalves, PMST de Castro, Application of the line spring model to some complex geometries, and comparison with three-dimensional results, *International Journal of Pressure Vessels and Piping* 76 (1999) 551-560
- [7] Goncalves JPM, de Castro PMST. Contribution to the numerical modeling of a corner crack at a fastener hole, SMAAC-WP-2.0-09-1.3/IDMEC (revised version), Brite-Euram Project No. BE95-1053, 1997.
- [8] A. Young, "Single-Domain Boundary Element Method for 3-D Elastostatic Crack Analysis", Document No. SMAAC-WP-2.0-07-1.0/DRA.
- [9] K-F. Nilsson, Accurate and reliable computation of stress intensity functions at corner cracks, FFA TN 1997-05, The Aeronautical Research Institute of Sweden, 1997.
- [10] C. Cali, R. Citarella, M. Perrella, Three-dimensional crack growth: numerical evaluations and experimental tests, *Biaxial/Multiaxial Fatigue and Fracture*, ESIS Publication 31, 2003, Ed. Elsevier, 341-360.
- [11] R. Citarella, M. Perrella, Multiple surface crack propagation: numerical simulations and experimental tests, *Fatigue and Fracture of Engineering Material and Structures* 28 (2005) 135-148.
- [12] C. Cali, R. Citarella, Residual strength assessment for a butt joint in MSD condition, *Advances in Engineering Software* 35 (2004) 373-382.
- [13] S.A. Sajjadi, S.M. Zebadjadk, Study of Fracture Mechanisms of a Ni-Base Superalloy at Different Temperatures, *Worldwide Journal of Achievements in Materials and Manufacturing* Vol. 18 (1-2), (2006) 227-230.
- [14] G. Mrówka-Nowotnik, J. Sieniawski, A. Nowotnik, Tensile properties and fracture toughness of heat treated 6082 alloy, *Worldwide Journal of Achievements in Materials and Manufacturing* Vol. 17 (1-2), (2006) 105-108.
- [15] M. Szutkowska, Modified indentation methods for fracture toughness determination of alumina ceramics, *Proceedings of AMME'2005*, Vol. 13 (2005) 651-654.
- [16] J. Hemanth, K.S. Shashi Shekar, Effect of heat transfer on strength and fracture behavior of Al/Al₂SiO₅/C hybrid MMCs, *Proceedings of AMME'2003*, Vol. 12 (2003).
- [17] R. Citarella, S. Gerbino, BE analysis of shaft-hub couplings with polygonal profiles, *Journal of Materials Processing Technology*, 109 (2001) 30-37.